# Plasma Cutting of Concrete: Heat Propagation and Molten Material Removal From the Kerf

Juan Camilo Chamorro, Leandro Prevosto, Ezequiel Cejas, Natalio Jorge Milardovich, Beatriz Rosa Mancinelli, and Gerardo Fischfeld

***Abstract*— An experimental investigation of heat propagation in the case of plasma cutting of concrete is reported. The experiments were carried out by using a high-enthalpy nitrogen plasma jet generated in a dc vortex-stabilized nontransferred arc torch. Concrete plates of different thicknesses up to 52 mm and with and without steel reinforcement were used. The plates were placed horizontally while cutting. The heat conduction losses inside the material were estimated by comparing thermocouple measurements and theoretical temperatures obtained with an analytical model of the heat propagation in the material. The influence of the molten concrete layer that separates the plasma to the solid material due to the high viscosity of the liquid concrete was accounted for. The power losses below the material in the extinguishing plasma have also been determined from calorimetric measurements. For different plate thicknesses and cutting velocities, a complete power balance of the process is performed with the calculation of the cutting efficiency on the basis of various relevant power terms. In addition, the hydrodynamics of the molten concrete layer in the kerf is analyzed. For a mean power level of 11.2 kW and a nitrogen gas flow rate of 25 Nl/min, the torch is able to cut a concrete plate of 52 mm in thickness with a speed of 20 mm/min and a whole efficiency of about 30%. The viscosity force is the main limiting factor on the cutting velocity in thick plates.**

***Index Terms*— Concrete, nontransferred arc torch, plasma cutting.**

## I. Introduction

PLASMA cutting is mostly used for electrical conductive materials. The plasma arc cutting process severs metal by using a constricted arc to melt a localized area of a workpiece (acting as the anode), removing the molten material with a high-velocity jet of plasma issuing from a constricting nozzle [1], [2]. Transferred arc plasma torches are widely used in the industrial cutting process of metallic materials because of their ability to cut practically all metal and the high productivity that can be achieved with this technology. In spite of this industrial development, there are only a few works concerning arc material interaction and heat transfer in the plasma cutting process (see [3] and references therein).

On the other hand, plasma cutting can also be extended to sever electrically nonconductive materials by using (noncurrent-carrying) plasma jets.

Atmospheric pressure thermal plasma jets generated in dc nontransferred arc plasma torches are used in a number of applications, such as plasma surface modifications, spray coatings, material synthesis, and waste treatment (see [4]–[8]). Standard dc nontransferred (spraying type) plasma torches operate with a central thoriated tungsten rod-type cathode and a water-cooled annular copper anode. The arc currents are in the range of a few hundred amperes. The torch voltage depends on the nature of the plasma gas and can vary between 20 and 30 V for atomic gases, up to 100 V or more when operating with molecular gases. As the gas passes around the arc through the anode-nozzle constriction, it is heated and partially ionized, emerging from the nozzle as a thermal plasma jet with a high specific enthalpy ranging between 5 and 35 MJ/kg in molecular gases. At the nozzle exit, the centerline value of the gas temperature is around 10 000–12 000 K (close to the electron one) and the velocity is of a few hundreds of meters per seconds [1]. The central core of the plasma jet is usually close to the local thermal equilibrium at atmospheric pressure (i.e., a "thermal plasma jet"), but large deviations from the LTE can exist in the peripheral zone due to rapid particle diffusion [4]–[6], [9].

The large number of possibilities for mixing, reinforcing, and using concrete in the construction industry is contrasted by only a few methods for pulling down and destroys old constructions. The oxygen thermal lance technique is the mainly used thermal cutting process for concrete and related materials in the construction industry [10], [11]. The process is characterized by the combustion of iron in an oxygen jet. Gas temperatures up to about 4000 K are obtained, thus imposing limitations on the heat flux carried out by the jet. It is, therefore, surprising that there are only very few papers [12] dedicated to investigate the feasibility of the thermal cutting of concrete and related materials through plasma jets. The improvement of this technology requires an advanced understanding of the process.

In this paper, an experimental investigation of heat propagation in the case of cutting of concrete by using a thermal plasma jet generated in a nontransferred arc torch operated

Manuscript received November 30, 2018; revised March 18, 2019; accepted April 29, 2019. Date of publication May 15, 2019; date of current version June 10, 2019. This work was supported in part by the Consejo Nacional de Investigaciones Científicas y Técnicas (CONICET) under Grant PIP 11220120100453 and in part by the Universidad Tecnológica Nacional under Grant PID 4626. The review of this paper was arranged by Senior Editor J. L. Lopez. *(Corresponding author: Juan Camilo Chamorro.)*

J. C. Chamorro, E. Cejas, N. J. Milardovich, and B. R. Mancinelli are with the Facultad Regional Venado Tuerto, Grupo de Descargas Eléctricas, Departamento Ing. Electromecánica, Universidad Tecnológica Nacional, Venado Tuerto 2600, Argentina (e-mail: jcchamorro@utp.edu.co).

L. Prevosto is with the Facultad Regional Venado Tuerto, Grupo de Descargas Eléctricas, Departamento Ing. Electromecánica, Consejo Nacional de Investigaciones Científicas y Técnicas (CONICET), Universidad Tecnológica Nacional, Venado Tuerto 2600, Argentina.

G. Fischfeld is with the Facultad de Ciencias Exactas, Ingeniería y Agrimensura (UNR), Santa Fe 2000, Argentina.

Color versions of one or more of the figures in this paper are available online at http://ieeexplore.ieee.org.

Digital Object Identifier 10.1109/TPS.2019.2914394

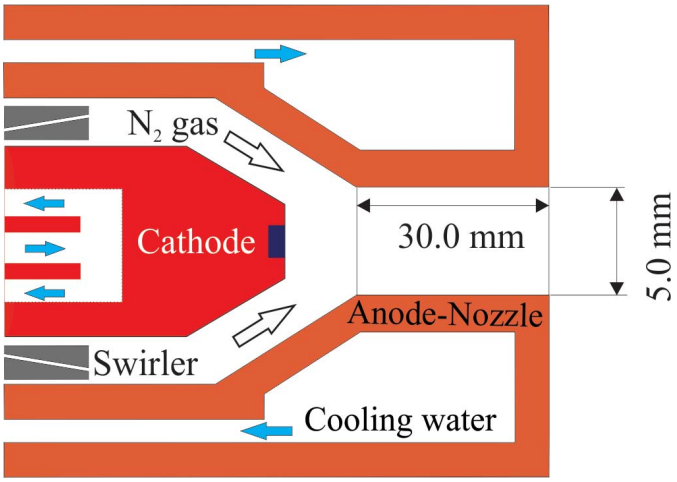


Fig. 1. Schematic of the nontransferred arc torch used in the experiments.

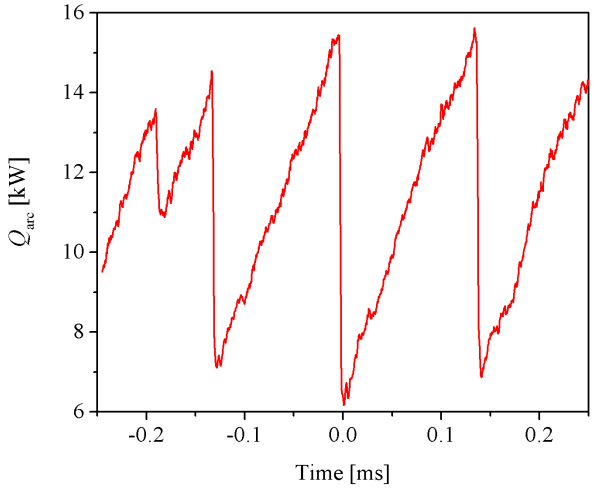


Fig. 2. Instantaneous arc power signal.

with nitrogen as the plasma gas is reported. The hydrodynamics of the molten concrete layer in the kerf is also analyzed. Section II presents the used experimental setup, while Section III describes the theory of heat diffusion in the material and power balance, as well as the hydrodynamics of the molten concrete. The results and its discussion are presented in Section IV. Section V summarizes the conclusion.

## II. Experimental Setup

### A. Nontransferred Vortex-Stabilized Arc Torch

The experiment was carried out using an atmospheric pressure nontransferred vortex-stabilized dc arc torch with a water-cooled thoriated tungsten (2 wt.%) rod-type cathode and a water-cooled copper anode nozzle of $D_n = 5$-mm internal diameter and 30 mm in length. A schematic of the employed arc torch is shown in Fig. 1. The torch was operated in the so-called restrike mode (see [6]) with a (measured) nitrogen flow rate of 25 Nl/min (corresponding to a mass flow rate $G = 0.47$ g/s). The arc voltage and discharge current were monitored on a Tektronix TDS 1002 B digital oscilloscope equipped with a high-voltage probe (Tektronix P6015A) and a current probe (Tektronix A622). The instantaneous arc power signal (obtained as the product of the discharge voltage and current) is shown in Fig. 2. The time-average arc power ($Q_{arc}$) was about 11.2 kW.

Two thermocouples, located at the inlet and outlet of the torch water cooling system, were used to measure the power lost from the arc to the cooling system ($Q_{wc}$). A temperature rise in the coolant water of about 20 °C was measured for a (measured) coolant flow rate of 3 L/min under the quoted torch operating conditions.

### B. Cutting Conditions

The operating conditions of the torch were fixed during the experiments ($Q_{arc} = 11.2$ kW and $G = 0.47$ g/s). The plates were placed horizontally while cutting. The distance between the nozzle exit and the top of the plates was also fixed at $h = 10$ mm. The cutting speed was varied from 20 to 26 mm/min, according to the plate thickness. A schematic of the whole experimental arrangement used for studying the heat transfer while cutting is shown in Fig. 3.

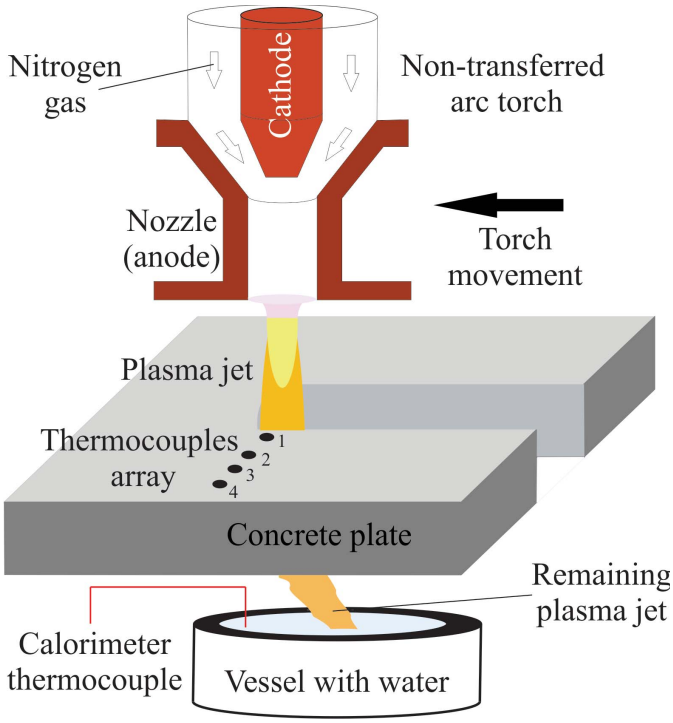


Fig. 3. Schematic of the whole experimental arrangement used to study the heat transfer while cutting.

### C. Thermocouples Array

For measurements inside the concrete, the temperature sensors were inserted into the plate (Fig. 3). Thermocouples were selected to this end as they are more robust than resistance temperature detectors and they can make measurement over a wider range of temperatures. Fast response K-type thermocouples (<1600 K), 1.5 mm in diameter, were used. The measurements were performed with an array of four thermocouples inserted into the concrete at the same depth (of half the thickness of the plate), perpendicularly to the kerf. A detailed schematic of the thermocouples array is shown in Fig. 4. The distance $d$ between the first thermocouple and the kerf was determined experimentally after each cutting. With this experimental configuration, it was possible to access heat

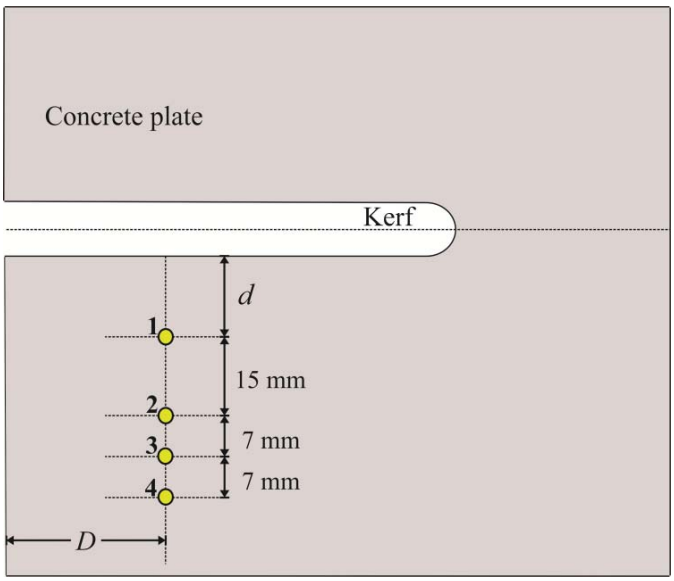


Fig. 4. Schematic of the thermocouples array inside a concrete plate.

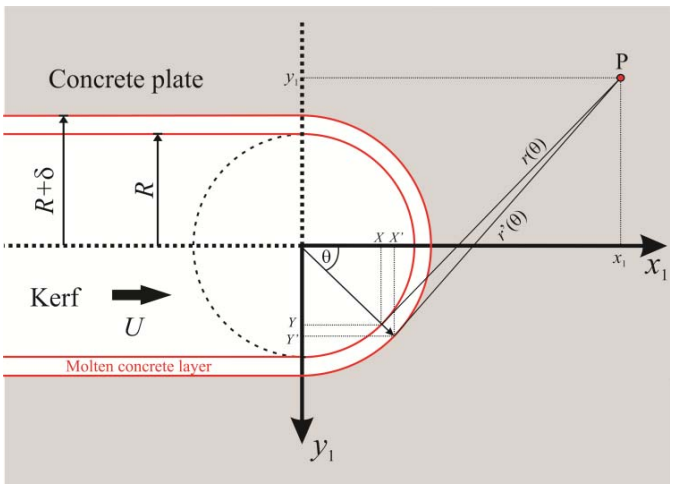


Fig. 5. Geometry used in calculations. Heat is delivered along the plasma-concrete boundary (hemi circle of radius $R$). The melting front has radius $R + \delta$.

conduction losses ($Q_{\text{diff}}$) inside the material by comparing the thermocouples experimental data with theoretical temperatures calculated on the basis of [13]–[15]; as it will be presented in the following section.

### *D. Calorimetric Technique*

Power losses below the material due to the remaining plasma jet enthalpy ($Q_{\text{re}}$) have been determined from calorimetric measurement in a vessel filled with water and positioned below the plate at the place of cutting (Fig. 3). The water temperature increase has been measured while cutting. The result calculations took into account the additional heat brought by the molten concrete ejected from the kerf by the plasma jet and collected at the bottom of the vessel.

### *E. Concrete Composition*

Concrete plates of different thicknesses $H = 25$, 32, and 52 mm, and with or without steel reinforcement, were used in the experiments. The composition of the used concrete is as follows: Portland cement is 446 kg/m$^3$, sand is 1051 kg/m$^3$, crushed stone aggregate is 1115 kg/m$^3$, and water is 301 kg/m$^3$. The concrete was reinforced by using an armature of steel bars of 5 mm in diameter with $50 \times 50$ mm mesh, embedded into the plates.

## III. Heat Diffusion in the Material, Power Balance, and Hydrodynamics of the Molten Concrete

### *A. Heat Propagation Model*

The arc power ($Q_{\text{arc}} = 11.2$ kW) is partially lost inside the torch, mainly through heating the torch electrodes. This loss approximately corresponds to the power transferred to the cooling water ($Q_{\text{wc}} = 4.2$ kW). The remaining part goes into plasma jet enthalpy ($Q_{\text{jet}} = 7$ kW), thus indicating an operating torch efficiency of about 62%.

Between the nozzle exit and the top of the plate, a part of this jet power is mainly lost through convection ($Q_{\text{lu}}$). The radiated power losses can be neglected in this case due to the relatively low average temperature of the plasma (see [16]). The rest corresponds to the available power brought by the jet inside the kerf ($Q_{\text{kerf}}$). The convection losses above the plate were estimated with the aid of the Nusselt number $N_u \equiv 0.023 \times R_e^{0.8} \times P_r^{0.3}$ [17], [18]; as $Q_{\text{lu}} = 2\pi h \lambda_{\text{pl}} T_{\text{pl}} N_u$ ($\lambda_{\text{pl}}$ and $T_{\text{pl}}$ are the plasma thermal conductivity and average temperature, respectively). The Reynolds number, based on the nozzle diameter and average plasma properties, $R_e \equiv \text{G}\nu_{\text{pl}}^{-1} D_n^{-1}$ ($\nu_{\text{pl}}$ is the kinematic viscosity of the plasma) is about 1000. The Prandtl number, $P_r \equiv \nu_{\text{pl}} \alpha_{\text{pl}}^{-1}$ ($\alpha_{\text{pl}}$ is the plasma thermal diffusivity), is about 0.7. The Nusselt number is $N_u \approx 5.5$. The plasma properties were taken from [1]. The power losses above the plate were finally estimated as $Q_{\text{lu}} \approx 0.2$ kW. The jet power reaching the kerf can then be estimated as $Q_{\text{kerf}} = 6.8$ kW.

To evaluate $Q_{\text{diff}}$, it is necessary to study theoretically and experimentally the heat propagation inside the material. The mathematical theory of heat distribution during welding and cutting has been first described in [13], and then was treated in a number of works (see [14]). In [14], heat transfer inside the workpiece during plasma arc cutting was based on the assumption that the molten metal is instantaneously removed from the kerf due to aerodynamic forces; i.e., no molten layer separates the plasma column and the solid metal. The effect of this liquid layer on the heat propagation was recently addressed in [15].

Because the viscosity $\mu$ of the molten concrete is very large, the concrete cannot be instantaneously removed from the kerf, and a liquid layer separating the plasma jet from the solid concrete should exists. Note that typical values of $\mu$ for molten concrete are $\mu \approx 1$–$0.1$ Pa·s [19], [20] for temperatures in the range of 1500–2200 K, i.e., about 100 to 1000 times higher than the viscosity of the molten steel ($\approx 3$–$5 \times 10^{-3}$ Pa·s [21]).

Under the present cutting conditions, the temperature distribution $T$ at any point $P$ in the material (see Fig. 5) is created not only by the heat sources at the plasma-concrete boundary (forward-directed half of the cylindrical jet column moving with a constant velocity $U$) but also by the heat sinks at the melting front that separates the liquid concrete from that not

yet molten. If the plate is large enough as compared to the extent of the heat source, the heat distribution around the heat source soon becomes constant, reaching the so-called "quasi-stationary" state [13] (i.e., the isotherms around the kerf will move at the same speed $U$ as the torch without undergoing any modification in the temperature field). This is justified if the characteristic Péclet number is significantly larger than unity. In addition, assuming that the heat sources and sinks are uniformly distributed, the temperature field in the plate is given by [15]

$$T(P)-T_\infty = \frac{Q_{\text{cut}}}{\pi^2\kappa H}\int_0^{\pi/2}\exp\left(-P_e\frac{x(\theta)}{2R}\right)\times K_0\left(P_e\frac{r(\theta)}{2R}\right)d\theta - \frac{Q_m}{\pi^2\kappa H}\int_0^{\pi/2}\exp\left(-P_e\frac{x'(\theta)}{2R}\right)\times K_0\left(P_e\frac{r'(\theta)}{2R}\right)d\theta \quad (1)$$

where $x(\theta)=x_1-X$, $r(\theta)=((x_1-X)^2+(y_1-Y)^2)^{1/2}$, $X=R\cos(\theta)$, $Y=R\sin(\theta)$, $x'(\theta)=x_1-X'$, $r'(\theta)=((x_1-X')^2+(y_1-Y')^2)^{1/2}$, $X'=(R+\delta)\cos(\theta)$, and $Y'=(R+\delta)\sin(\theta)$ ($x_1$, $y_1$ are the coordinates of the point $P$ measured from the reference frame moving with the torch.) $Q_{\text{cut}}$ is the jet power transferred to the material, $R$ is the average half-width of the kerf (the plasma jet radius), and $\delta$ is the average width of the liquid layer. $T_\infty$ is the material temperature far from the kerf (= 300 K), and $\kappa$ and $\alpha$ are the concrete thermal conductivity and thermal diffusivity, respectively. $P_e \equiv \text{UR}\alpha^{-1}$ is the Péclet number. $K_0$ is the zero-order and the second kind of modified Bessel function [22]. The average half-width of the kerf and the width of the liquid layer were measured after each cutting, the latter was estimated by measuring the average thickness of the rapidly resolidified molten concrete layer at the edge of the kerf. $Q_m$ is the power involved in the melting of concrete [15]

$$Q_m = \pi\rho(R+\delta)U\left\{\int_{T_\infty}^{T_m}C(T)dT+L_m\right\} \quad (2)$$

where $\rho$ and $C(T)$ are the concrete density and heat capacity, respectively. $L_m$ is the latent heat of fusion and $T_m$ is the temperature melting point of the concrete.

The heat diffusion inside the workpiece ($Q_{\text{diff}} \equiv Q_{\text{cut}}-Q_m$) can be calculated by varying $Q_{\text{cut}}$ in (1) to find the best agreement between the theoretical temperatures and thermocouples measurements. However, it should be noted that the homogeneous and uniform heat transfer along the whole thickness of the plate is probably not completely justified. In addition, thermal conductivity and diffusivity in (1) are supposed to be constant with temperature, which is a crude approximation.

The values of thermal conductivity and thermal diffusivity at a high temperature corresponding exactly to the concrete composition used during the experiments were not found in the literature. Furthermore, the physical properties of concretes at high temperature (close or above the melting point) are scarce [19], [20], [23]. Average values of appropriate concrete thermal properties for various compositions are: $\rho$ = 2300–2600 kg m$^{-3}$, $\kappa$ = 0.5–3 W·m$^{-1}$ K$^{-1}$, $\alpha$ = 2–10 × 10$^{-7}$ m$^2$·s$^{-1}$, and $L_m$ = 1–2 MJ·kg$^{-1}$, for solid concrete; and

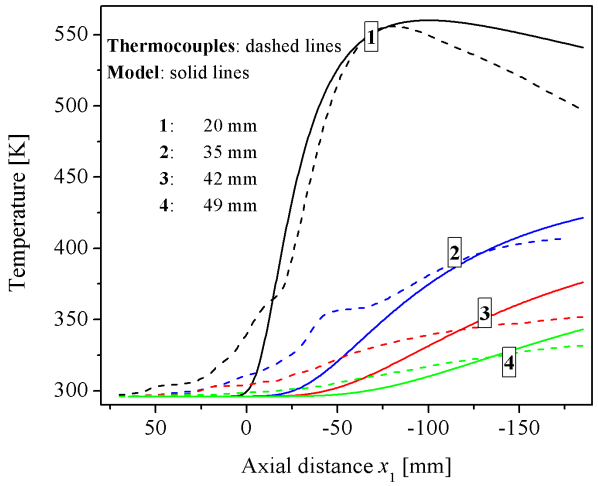


Fig. 6. Theoretical and experimental temperatures distributions inside the workpiece. ($H$ = 25 mm, $d$ = 15 mm, and $R$ = 5 mm). The radial positions ($y_1$) of the thermocouples are also shown.

$\rho$ = 2200–2600 kg m$^{-3}$, $\kappa$ = 1–1.2 W m$^{-1}$ K$^{-1}$ and $\alpha$ = 3 × 10$^{-7}$ m$^2$ s$^{-1}$, for molten concrete ($T_m$ = 1300–1800 K). The following values were used in this paper: $\kappa$ = 2 W·m$^{-1}$·K$^{-1}$ and $\alpha$ = 6 × 10$^{-7}$ m$^2$·s$^{-1}$. These two coefficients correspond to average values in the temperature range 300–600 K, which typically correspond to the temperatures measured by the thermocouples (Fig. 6). In order to evaluate the influence of these parameters on the model results, a series of calculations was performed with different $\kappa$ and $\alpha$ values. A modification of $\kappa$ up to ±25% induces a 5% maximum variation in $Q_{\text{cut}}$. The effect of $\alpha$ is somewhat higher: a change of ±25% produces a $Q_{\text{cut}}$ deviation of less than 10%. Moreover, as the heat capacity and thermal conductivity vary in the opposite way with temperature [23], their effects are partially compensated, and the diffusivity does not significantly vary in the temperature range 300–600 K.

The power losses beneath the material mainly correspond to the residual enthalpy in the extinguishing plasma jet ($Q_{\text{ep}}$) and the power involved in superheating the molten concrete ($Q_{\text{sh}}$). Note that $Q_{\text{ep}}$ can be estimated from calorimetric measurement, while the power term $Q_{\text{sh}}$ has to be estimated by realizing a global power balance of the cutting process ($Q_{\text{sh}} = Q_{\text{kerf}}-Q_{\text{cut}}-Q_{\text{ep}}$).

With the power balance, it is possible to calculate two different efficiencies. The first one is the efficiency $\eta$ of the whole process, corresponding to the ratio between the power involved in the melting of concrete $Q_m$, and the total power provided by the arc $Q_{\text{arc}}$. The second one is the kerf efficiency, $\eta_k$, defined as the ratio between the power effectively involved in melting $Q_m$ and $Q_{\text{cut}}$.

### *B. Hydrodynamics of the Molten Concrete Layer in the Kerf*

The plasma jet melts a mass$\rho\pi$ $(R+\delta)$ $HU$ of the concrete per second that leaves the bottom of the plate with a velocity $v$. This speed can be estimated from the law of mass conservation, as $v = \text{UH}\delta_b^{-1}$. $\delta_b$ is the width of the liquid layer at the bottom of the plate. $\delta = 1/2\delta_b$ for a liquid layer width increasing linearly along the thickness of the plate.

The momentum flux carried by the molten concrete leaving the plate is $\rho\pi\ (R+\delta_b)\delta_b v^2$.

Several forces act on the liquid layer [24] are as follows.

1) The aerodynamic force $F_{\text{drag}} = \tfrac{1}{2}G^2\rho_{\text{pl}}^{-1}C_f H\pi^{-1}R^{-3}$, arising due to the jet friction (drag) over the much more slow motion of the melt, that pushes the liquid material downward. $\rho_{\text{pl}}$ is the average plasma density and $C_f$ is the drag coefficient (depending on the Reynolds number).
2) The gravity force $F_{\text{gravity}} = \rho g\pi\ (R+\delta)\delta H$ ($g$ is the acceleration of gravity) that also pushes the liquid material downward.
3) The surface tension force $F_{\text{surface-tension}} = \gamma\,\pi\ (R+\delta)$, (where $\gamma$ is the surface tension coefficient of the molten concrete) that slows down the movement of the liquid layer.
4) The viscosity force $F_{\text{viscosity}} = \mu v\delta^{-1}\pi\ (R+\delta)H$ that also slows down the movement of the liquid layer.

The sum of all the above-entioned forces accelerates the molten concrete. According to the momentum conservation law

$$\frac{G^2C_fH}{2\pi R^3\rho_{pl}} + \rho g\pi\delta H(R+\delta) - \gamma\pi(R+\delta) - \mu\frac{v}{\delta}\pi(R+\delta)H = \rho\pi\delta_b(R+\delta_b)v^2. \quad (3)$$

The average thickness $\delta$ of the liquid layer can then be obtained from (3). However, not all the forces acting on the liquid layer are equally important, as it will be shown in the next section.

## IV. Experimental Results and Discussion

### *A. Thermocouples and Calorimetric Measurements: Power Balance*

An example of thermocouples measurements inside a concrete plate is given in Fig. 6 as a function of the axial distance $x_1$ (see Fig. 5), for the following cutting conditions: plate thickness $H = 25$ mm and torch velocity $U = 26$ mm/min. For comparative purposes, theoretical temperatures calculated with (1) were also shown in Fig. 6. Note that the thermocouple recorded temperatures are time-dependent, but, with the assumption of a "quasi-stationary" state, and the knowledge of cutting speed and the distance $D$ between the thermocouples array and the plate edge (as shown Fig. 4), a coordinate change: time $\rightarrow$ space ($x_1$) was operated [25] (the Péclet number characterizing the transport of heat in the plates is about 3–10). The best agreement between the experimental and model results for the concrete plate of 25 mm in thickness was obtained when the power transferred to the concrete is fixed at $Q_{\text{cut}} = 3200$ W. Considering the simplifications assumed in the analytical model [15], the agreement between the experimental and calculated temperatures (within $\pm 15\%$) is satisfactory. There are several possibilities to explain the discrepancies. First, the thermal properties of the concrete are supposed to be constant with the temperature. This assumption could introduce some modifications in the temperature field. Second, the thermocouples inserted into the concrete plate induce inhomogeneities which could also modify conduction properties of the material with temperature. Finally, the thermal properties values corresponding exactly to the concrete composition used during the experiments were not found in the literature; hence, the appropriate characteristic values were used.

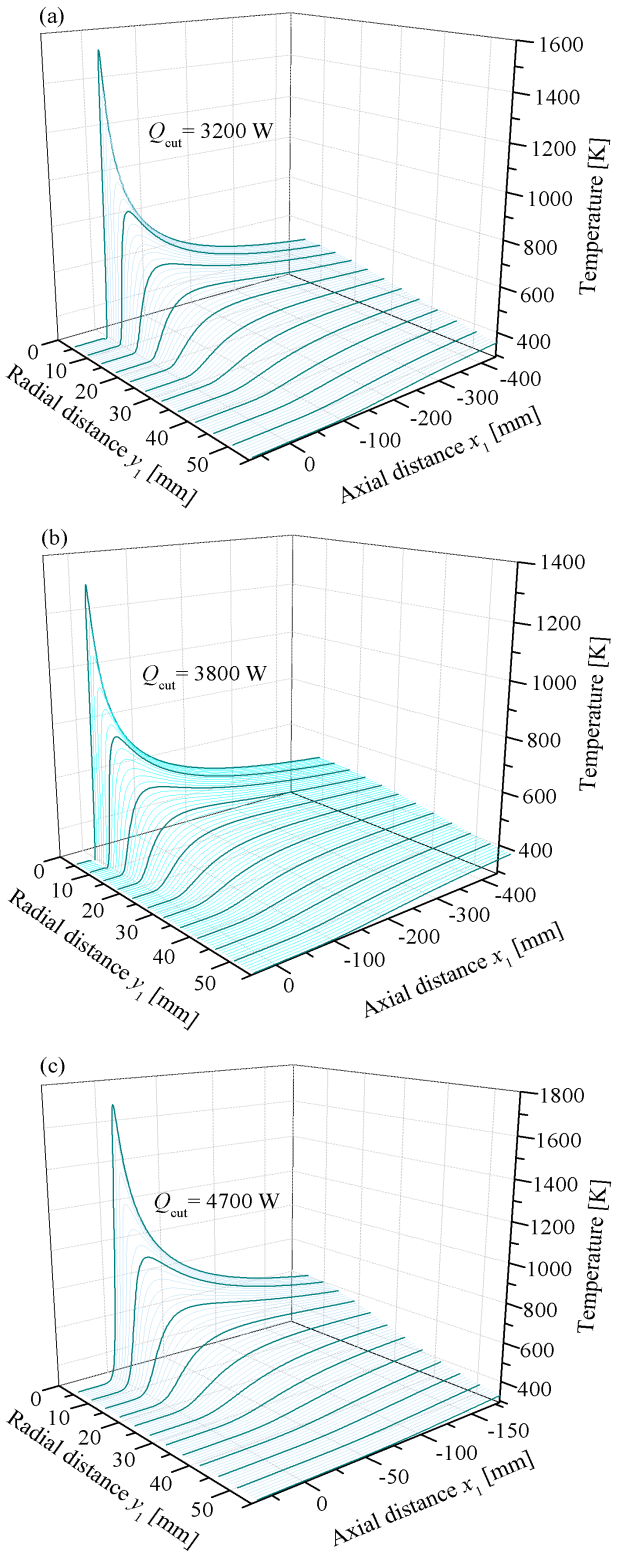


Fig. 7. Theoretical temperature distributions: (a) $H = 25$ mm, (b) $H = 32$ mm, and (c) $H = 52$ mm.

For the other sets of cutting parameters ($H = 32$ mm and $U = 24$ mm/min; and $H = 52$ mm and $U = 20$ mm/min), thermocouples measurements have also been used to reconstitute the temperature field inside the concrete plates. Again, a good correspondence between the experimental (not showed) and calculated temperatures was observed. The model results are shown in Fig. 7. Fig. 7(a) shows the calculated temperature distribution for the plate of $H = 25$ mm. For the plate of 32 mm in thickness, as shown in Fig. 7(b), the best accuracy is obtained with $Q_{\text{cut}} = 3800$ W, while for the thicker plate, as shown in Fig. 7(c), the best accuracy is obtained with $Q_{\text{cut}} = 4700$ W. As expected, the material temperature close to the kerf-front ($\approx$ 1300–1700 K) results in all the cases close to the temperature melting point of the concrete. Large temperature gradients are observed close to the kerf due to the small thermal diffusivity of the concrete.

For the thermocouples temperature measurements, only concrete plates without steel reinforcement were used.

The average half-width of the kerf as well as the average width of the molten concrete layer were measured during the experiments to estimate the amount of removed material for the $Q_m$ power term evaluation. The latter was inferred by measuring the width $\delta_b$ of the liquid layer at the bottom of the plate, namely, $\delta = ½\delta_b$. Both kerf parameters do not show noticeable variations with the concrete plate thickness, with average values of about $R = 4$–5 mm and $\delta_b \approx 1$ mm.

In addition, observations show that the angle of declination of the walls of the cut from the vertical (the so-called bevel angle) is quite small (i.e., the walls of the cut are almost vertical under the present conditions). It is important to note for the case of cutting metals with arc plasmas that the walls of the cut are never vertical (typically the top is wider than its bottom). Furthermore, it was demonstrated that as the cutting speed increases, the kerf width at the plate bottom decreases (bevel angle increases), which is the general rule [2], [3]. The aforementioned suggests that the squareness of the cut for the case of plasma cutting of concrete could be related with the low velocity of the cutting process (20–26 mm/min), imposed by hydrodynamic phenomena in the liquid concrete layer inside the kerf (as shown Fig. 10). Heat conduction losses $Q_{\text{diff}}$, the power involved in melting the concrete $Q_m$, the losses beneath the material due to the plasma residual enthalpy $Q_{\text{ep}}$, and the power term involved in superheating the molten concrete $Q_{\text{sh}}$ are reported in Fig. 8. The cutting speed is also shown.

Although systematic studies varying the torch velocity were not performed, observations of the backward deflection of the jet under the plates during the experiments suggest that the reported cutting velocities (20 to 26 mm/min) are not far from the maximum for the given torch operating conditions. These velocity values are consistent with those reported in the experiment [12].

Note from Fig. 8 that $Q_m$ and $Q_{\text{diff}}$ exhibit more or less the same behavior while varying the plate thickness, thus indicating that the power involved in melting and heat conduction losses are part of a single power term corresponding to the power deposited inside the material $Q_{\text{cut}}$. The existence of a proportionality relation between $Q_m$ and $Q_{\text{diff}}$

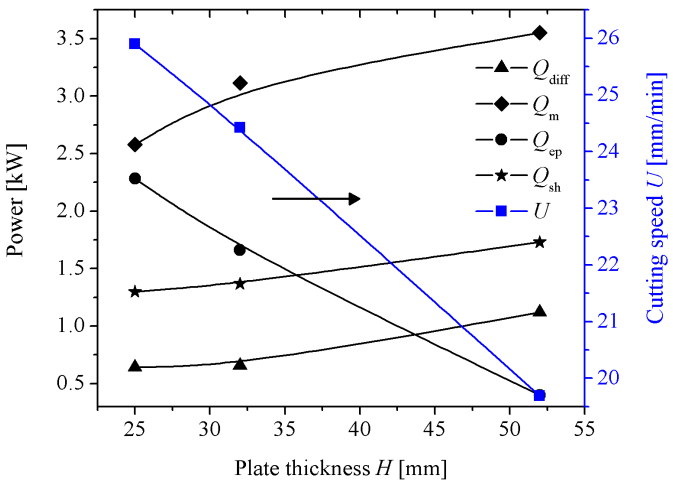


Fig. 8. Power terms involved inside the kerf and cutting velocity as functions of the thickness of the concrete plates.

was also found in the plasma arc cutting process [25], [26]. In [25], the experimentally inferred value of the power lost into the metal through thermal conduction was as high as 80% of the power involved in melting. However, under the present conditions, due to the small thermal diffusivity of the concrete as compared with the steel, the heat does not deeply penetrate into the concrete, and a large fraction of the power transferred to the material is used in melting the concrete. That is, the power lost into the concrete plate due to thermal conduction reaches only about 25%–30% of the power required for melting, namely, the kerf efficiency $\eta_k$ reaches a value about 75%–80% under the present conditions.

A significant decrease in (the measured) power losses under the plate $Q_{\text{ep}}$ is also observed with increasing the plate thickness in Fig. 8. This behavior is related to the increases in the power deposited inside the material $Q_{\text{cut}}$ at constant arc power. The power involved in superheating the molten concrete $Q_{\text{sh}}$ follows the trend of the power involved in melting while varying the plate thickness. This result is evident since both $Q_m$ and $Q_{\text{sh}}$ are directly proportional to the melting rate that increases with the plate thickness. Note that the superheating of the molten concrete could improve the material removal from the kerf by reducing the viscosity [12]. This behavior is related to the strong (exponential) decay of the viscosity of the liquid concrete with the temperature, at values above (but close) to the melting point [27].

The whole efficiency $\eta$ of the cutting process was also calculated. The value varies from about 25% to 30% while varying the plate concrete thickness from 25 to 52 mm, respectively. Note from the basis of the above presented results that the power balance in the case of the plasma cutting of concrete can be adequately described by a simple model in which the input heat is mainly consumed by the process of concrete melting (i.e., by neglecting $Q_{\text{diff}}$ due to the low thermal diffusivity of the concrete).

### *B. Molten Concrete Removal From the Kerf*

For all the investigated cutting parameters, the plasma jet was able to produce defined cuts in the concrete plates regardless of the steel reinforcement. For instance, Fig. 9 shows a

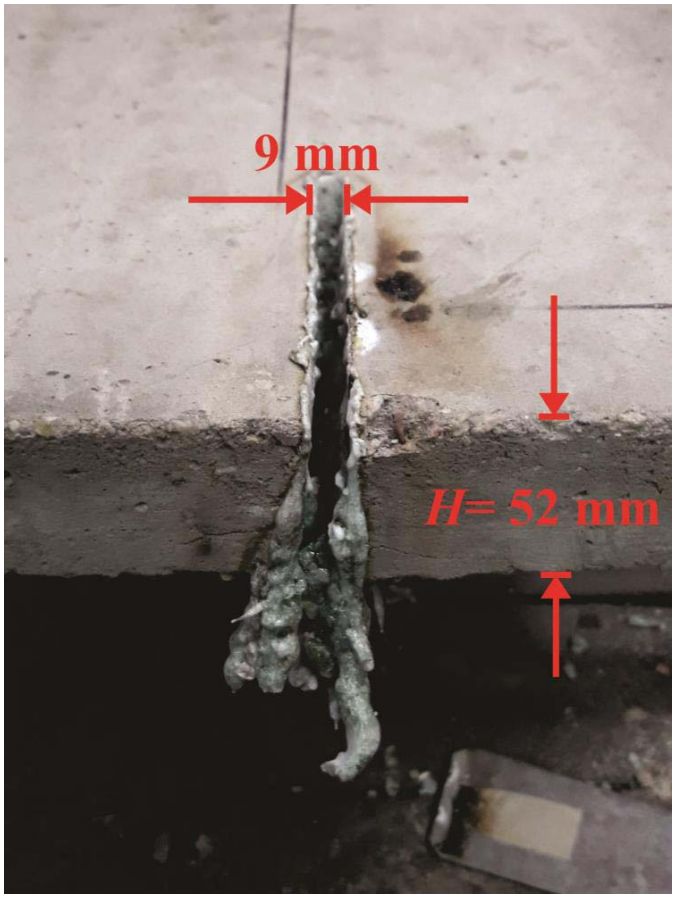


Fig. 9. Photograph of a typical kerf in a concrete plate after the plasma cutting ($H = 52$ mm).

typical kerf in a concrete plate of 52 mm after the experiments. The dross (resolidified concrete removed from the kerf adhering to the bottom of the plate) is also shown. Note that the presence of steel reinforcement could improve the expulsion of the molten concrete from the kerf, as it reduces the viscosity of the mixture.

An evaluation of the thickness of the molten concrete was obtained according to (3). The calculated $\delta$ values, together with the relative importance of the gravity on the molten concrete on the basis of the obtained the experimental data, are presented in Fig. 10. The following concrete properties were used [19], [20], [23]: $\rho = 2500$ kg·m$^{-3}$, $\eta = 0.3$ Pa·s, and$\gamma = 0.3$ N·m$^{-1}$. $R = 4$ mm. ($C_f = 0.01$ for $R_e = 1000$–$2000$ [28]). As shown in Fig. 10, the calculated average thickness values of the molten concrete layer ($\delta \approx 0.5$ mm) are in good correspondence with those experimental inferred.

According to Fig. 10, the main forces that oppose the removal of molten concrete from the kerf are the viscosity and surface tension. The importance of viscosity depends on the thickness of the plate. The thicker the plate, the greater the role of the viscosity. The removal of the molten concrete is mainly due to gravity. The aerodynamic drag plays a minor (but not negligible) role compared to gravity. The reason is the rather low momentum flux carried by the plasma jet issuing from the wide nozzle at the above torch operating conditions.

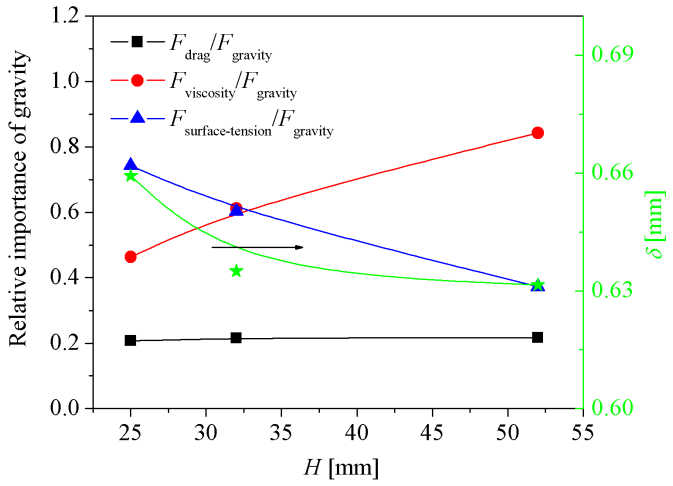


Fig. 10. Relative importance of the gravity for cutting of concrete and thickness of the molten concrete layer, according to the hydrodynamic model.

As the viscosity force is proportional to the molten concrete velocity ($v = UH\delta_b^{-1}$), it imposes restrictions on the cutting velocity: in thick plates, the cutting velocity must be so small that the viscosity almost completely balances the gravity (i.e., inertia is completely negligible in this limiting case). The molten concrete moves downward with nearly constant and low ($v \approx 1$–$2$ cm/s) velocity.

Contrarily, in the plasma arc cutting process (cutting velocities in the range 700–5000 mm/min), the main slowing force is the surface tension (higher in a factor about four than that of the molten concrete [20], [21]). The effect of the relatively low viscosity is negligible. However, the aerodynamic drag force is balanced only partially by the surface tension: the molten steel is accelerated continuously from the top to the bottom of the plate due to the high-velocity arc jet issuing from a constricting nozzle. The movement is inertia controlled. The gravity is significant only in the case of cutting very thick plates [2], [24].

No vertical cuts were investigated in this paper. However, the above model can be used to analyze the hydrodynamic of the molten concrete layer in vertical cuts under the experimental conditions of [12]: $U = 20$ mm/min, $H = 120$ mm, plasma gas nitrogen, $G = 1.5$ g/s, and $Q_{\text{arc}} = 35$ kW. The calculations show that the aerodynamic force is almost balanced by the viscosity. The surface tension has a minor role and the inertia is completely negligible, i.e., the movement of the liquid concrete is viscosity controlled. ($R = 4$–$5$ mm and $\delta_b \sim 1$ mm were used in the calculations). Unfortunately, at present, the experimental data on plasma cutting of concrete and related materials are reduced to the results in [12]. Therefore, no other comparison with published results is possible.

The hydrodynamic model results shown in Fig. 10 seem to be supported by the experiments. Note from Fig. 9 that the molten concrete is effectively removed from the kerf, but the presence of heavy dross suggests that it flows downward at low velocity, so that the adhesion of the molten concrete takes place at the bottom of the plate to form the dross. In addition, it was found that at a further increase in the cutting velocities

yields a sharp increase in the backward deflection angle of the plasma jet under the plate, thus suggesting that the reported cutting velocities are not far from the limiting velocities. Furthermore, the calculated average thickness values of the molten concrete layer for different cutting conditions are in good correspondence with those experimental inferred.

## V. Conclusion

Thermocouples measurements of the temperature field inside concrete plates while cutting with a (spraying type) plasma torch operating with nitrogen as plasma gas were performed. The plates were placed horizontally during the experiments. Calorimetric measurements of the remaining enthalpy in the extinguishing plasma jet under the plates were also carried out. A complete power balance of the cutting process was presented. In addition, the hydrodynamics of the high-viscosity molten concrete layer in the kerf was analyzed. The results have shown the following.

1) The nitrogen plasma jet is capable of producing localized cuts in concrete. For a mean power level of 11.2 kW, and a nitrogen gas flow rate of 25 Nl/min, the torch was able to cut a concrete plate of 52 mm in thickness with a speed of 20 mm/min.
2) The whole efficiency of the plasma cutting process varies from about 25% to 30% while varying the plate thickness from 25 to 52 mm, respectively.
3) Due to the small thermal diffusivity of the concrete, the power lost into the plate due to thermal conduction reaches only about 25%–30% of the power required for melting. Correspondingly, the kerf efficiency reaches values in the range of 75%–80% under the present conditions.
4) The main forces that oppose the removal of the molten concrete from the kerf are the viscosity and surface tension. The removal of the molten concrete is mainly due to gravity. The aerodynamic drag plays a minor role due to the rather low momentum flux carried by the plasma jet for the operating conditions of the torch. The importance of the viscosity grows with the plate thickness, thus imposing restrictions on the cutting velocity: in thick plates, the cutting velocity must be so small that the viscosity almost completely balances the gravity. Inertia is completely negligible in this limiting case. These results are supported by the experimental data found.

## Acknowledgment

L. Prevosto is a member of the Consejo Nacional de Investigaciones Científicas y Técnicas (CONICET). J. C. Chamorro and E. Cejas would like to thank CONICET for their doctoral fellowships.

## References

[1] M. I. Boulos, P. Fauchais, and E. Pfender, *Thermal Plasmas: Fundamentals and Applications*, vol. 1. New York, NY, USA: Plenum, 1994.
[2] V. A. Nemchinsky and W. S. Severance, "What we know and what we do not know about plasma arc cutting," *J. Phys. D: Appl. Phys.*, vol. 39, no. 22, pp. R423–R438, Nov. 2006.
[3] V. Nemchinsky, "Heat transfer in plasma arc cutting," in *Handbook of Thermal Science and Engineering*, F. A. Kulacki, Ed. Cham, Switzerland: Springer, 2018, pp. 2729–2790.
[4] P. Fauchais and A. Vardelle, "Thermal plasmas," *IEEE Trans. Plasma Sci.*, vol. 25, no. 6, pp. 1258–1280, Dec. 1997.
[5] P. Fauchais and A. Vardelle, "Pending problems in thermal plasmas and actual development," *Plasma Phys. Controlled Fusion*, vol. 42, no. 12B, pp. 365–383, Dec. 2000.
[6] P. Fauchais, "Understanding plasma spraying," *J. Phys. D: Appl. Phys.*, vol. 37, no. 9, pp. 86–108, 2004.
[7] A. Vardelle, C. Moreau, N. J. Themelis, and C. Chazelas, "A perspective on plasma spray technology," *Plasma Chem. Plasma Process.*, vol. 35, no. 3, pp. 491–509, May 2015.
[8] A. Vardelle *et al.*, "The 2016 thermal spray roadmap," *J. Therm. Spray Technol.*, vol. 25, no. 8, pp. 1376–1440, Dec. 2016.
[9] J. C. Chamorro, L. Prevosto, E. Cejas, and H. Kelly, "Quantitative schlieren diagnostic applied to a nitrogen thermal plasma jet," *IEEE Trans. Plasma Sci.*, vol. 47, no. 1, pp. 473–482, 2018. doi: 10.1109/TPS.2018.2869031.
[10] R. D. Woodson, *Concrete Structures*, 1st ed. Oxford, U.K.: Butterworth-Heinemann, 2009.
[11] A. Bargagliotti, L. Caprile, F. Piana, and E. Tolle, "Plasma arc and thermal lance techniques for cutting concrete and steel," Nuclear Sci. Technol., Commission Eur. Communities, Brussels, Belgicum, Tech. Rep. EUR 10402 EN, 1986.
[12] B. Dzur, W. Rother, G. Nutsch, J. Schilling, and A. Schwarze, "Thermal cutting of concrete and related materials," *Ann. New York Academy Sci.*, vol. 891, no. 1, pp. 223–230, Dec. 1999.
[13] D. Rosenthal, "The theory of moving sources of heat and its application of metal treatments," *Trans. ASME*, vol. 68, no. 8, pp. 849–866, Nov. 1946.
[14] V. Nemchinsky, "Dross formation and heat transfer during plasma arc cutting," *J. Phys. D: Appl. Phys.*, vol. 30, no. 18, pp. 2566–2572, Sep. 1997.
[15] V. Nemchinsky, "Temperature created by a moving heat source that heats and melts the metal plate (plasma arc cutting)," *J. Heat Transf.*, vol. 138, no. 12, Aug. 2016, Art. no. 122301.
[16] Y. Naghizadeh-Kashani, Y. Cressault, and A. Gleizes, "Net emission coefficient of air thermal plasmas," *J. Phys. D: Appl. Phys.*, vol. 35, no. 22, pp. 2925–2934, 2002.
[17] W. H. McAdams, *Heat Transmission*, 3rd ed. New York, NY, USA: McGraw-Hill, 1954.
[18] A. R. Dayal and R. T. Deam, "Maximum plasma power for a cylindrical bore torch," *J. Phys. D: Appl. Phys.*, vol. 35, no. 13, pp. 1486–1490, Jun. 2002.
[19] K. Pentillä, "Molten corium and concrete thermodynamics and viscosity," VTT Tech. Res. Centre, Espoo, Finland, Res. Rep. VTT-R-01441-12, Feb. 2012.
[20] A. S. Benjamin, "Core-concrete molten pool dynamics and interfacial heat transfer," in *Proc. ANS/ASME Top. Meeting Nucl. React. Therm. Hydraul.*, New York, NY, USA, vol. 2, 1980, pp. 1–30.
[21] N. Christensen *et al.*, "The physical properties of fluids at elevated temperatures," in *The Physics of Welding*, F. Lancaster, Ed. New York, NY, USA: Pergamon Press, 1986, pp. 9–46.
[22] F. W. J. Olver, "Bessel function of integer order," in *Handbook of Mathematical Functions*, M. Abramowitz and I. A. Stegun, Eds. New York, NY, USA: Dover, 1972, pp. 355–389.
[23] R. J. McNamee, P. Pimienta, and R. Felicetti, "Thermal properties," in *Physical Properties and Behaviour of High-Performance Concrete at High Temperature*, P. Pimienta, R. J. McNamee, R. Mindeguia, and J. Christophe, Eds. Cham, Switzerland: Springer, 2019, pp. 61–69.
[24] V. A. Nemchinsky, "Liquid metal movement during plasma arc cutting," *Weld. J.*, vol. 75, no. 12, pp. 388s–392s, Dec. 1996.
[25] P. Teulet *et al.*, "Experimental study of an oxygen plasma cutting torch: II. Arc–material interaction, energy transfer and anode attachment," *J. Phys. D: Appl. Phys.*, vol. 39, no. 8, pp. 1557–1573, Mar. 2006.
[26] S. Ramakrishnan, V. Shrinet, F. B. Polivka, T. N. Kearney, and P. Koltun, "Influence of gas composition on plasma arccutting of mild steel," *J. Phys. D: Appl. Phys.*, vol. 33, no. 18, pp. 2288–2299, Sep. 2000.
[27] Y. Ohishi, F. Kargl, F. Nakamori, H. Muta, K. Kurosaki, and S. Yamanaka, "Physical properties of core-concrete systems: $Al_2O_3$-$ZrO_2$ molten materials measured by aerodynamic levitation," *J. Nucl. Mater.*, vol. 487, pp. 121–127, Apr. 2017.
[28] F. M. White, *Fluids Mechanics*, 4th ed. New York, NY, USA: McGraw-Hill, 2001.

**Juan Camilo Chamorro** was born in Riosucio, Colombia, in 1989. He received the Engineering degree in physics engineering from Pereira Technological University, Pereira, Colombia, in 2013.

Since 2014, he has been a Doctoral Fellow with the Consejo Nacional de Ciencias y Tecnología (CONICET), Venado Tuerto, Argentina. He is currently conducting Ph.D. studies with the Electrical Discharge Group, National Technological University, Rosario, Argentina, and the Faculty of Engineering, Rosario National University, Rosario. His current research interests include plasma diagnostic and computational modeling of thermal and nonthermal discharges.

**Leandro Prevosto** was born in Venado Tuerto, Argentina, in 1971. He received the Diploma degree in electromechanical engineering from the National Technological University, Rosario, Argentina, in 2005, and the Ph.D. degree in engineering from the University of Buenos Aires, Buenos Aires, Argentina, in 2009.

Since 2010, he has been a Professor with National Technological University, where he is currently with the Electrical Discharge Group. Since 2012, he has been a Researcher with the Consejo Nacional de Ciencias y Tecnología (CONICET), Venado Tuerto, Argentina. His current research interests include thermal and nonthermal electrical discharges, plasma diagnostics, and plasma applications.

**Ezequiel Cejas** was born in Los Quirquinchos, Argentina, in 1987. He received the Engineering degree in electromechanical engineering from Venado Tuerto Regional Faculty, National Technological University, Venado Tuerto, Argentina, in 2017.

Since 2017, he has been a Doctoral Fellow with the Consejo Nacional de Ciencias y Tecnología (CONICET), Venado Tuerto. He is conducting Ph.D. studies with the Electrical Discharge Group, National Technological University, Rosario, Argentina, and the Faculty of Engineering, Rosario National University, Rosario. His current research interests include optical diagnostics, numerical modeling, and plasma technology.

**Natalio Jorge Milardovich** was born in Chovet, Argentina, in 1959. He received the Diploma degree in electrical engineering from National Technological University, Rosario, Argentina, in 1986, and the master's degree in energy for sustainable development from the National University of Rosario, Rosario, in 2015.

Since 1987, he has been a Professor with National Technological University, where he has been with the Electrical Discharge Group since 2012. His current research interests include thermal and nonthermal electrical discharges, plasma diagnostics, and plasma applications.

**Beatriz Rosa Mancinelli** was born in Santa Fe, Argentina, in 1965. She received the Ph.D. degree in nuclear engineering from the Balseiro Institute, Bariloche, Argentina, in 1990, and the Ph.D. degree from National Technological University, Rosario, Argentina, in 2010.

Since 2010, she has been a Professor with National Technological University, where she has been a Researcher with the Electrical Discharge Group, since 2012. His current research interests include numerical modeling of thermal and nonthermal electrical discharges, and plasma applications.

**Gerardo Fischfeld** was born in Buenos Aires, Argentina, in 1950. He received the Ph.D. degree in physics and the Ph.D. degree from the National University of Rosario, Rosario, Argentina, in 1978 and 1986, respectively.

Since 1991, he has been a Professor with the National University of Rosario. He was involved in plasma physics, plasma optical diagnostics, high-power lasers, high-power radio frequency oscillators, small nuclear power reactors, and cyclotrons of 11 and 42 MeV. His current research interests include the characterization and growth of KDP-type crystals, thermal and nonthermal electrical discharges, plasma diagnostics, and high-power electronic devices.